

Interaction potential of FePt with the MgO(001) surface

R. Cuadrado and R. W. Chantrell

Department of Physics, University of York, York YO10 5DD, United Kingdom

(Received 9 December 2014; published 19 February 2015)

By means of density functional theory we have undertaken a structural, electronic, and magnetic survey of the adsorption of the Fe_xPt_y ($x, y \leq 4$) clusters on the MgO(001) surface under the generalized gradient approximation. We have tested different atomic adsorption geometries with the aim of scanning a wider range of adsorption sites in order to determine the preferential surface covering. The *intracluster* (before and after the adsorption) and cluster-to-surface binding mechanisms were investigated via the adsorption energy, charge transfer, density of states, and hybridization analysis. The adsorption energy values increased for those geometries in which keeping the Fe or Pt atom @*top*-O, and the outermost species was moved to *cover* the surface. In general the unsupported clusters present higher *intracluster* energies than the adsorbed ones with an average difference of 1.5 eV. In this regard there was a small reduction in the net magnetic moment of the supported clusters due to an internal and external rearrangement of the spin-up/-down charge. Furthermore, a complex and subtle charge transfer between different species takes place having an increase in the Pt and O population at the expense of the lost Fe charge.

DOI: [10.1103/PhysRevB.91.075420](https://doi.org/10.1103/PhysRevB.91.075420)

PACS number(s): 75.50.Ss, 71.15.Nc, 31.50.Bc

I. INTRODUCTION

During the past two decades, continuous miniaturization has driven data-storage technology to the nanometer scale, and consequently, the study of magnetism in low-dimensional systems is currently attracting a great deal of interest [1,2]. The interaction of metallic clusters and alloys with supporting metal-oxide surfaces is the subject of great current interest because of their numerous technological applications [3,4]. Important objectives of these studies are to understand how the atomic and electronic structures of both subsystems are modified through their interaction as well as the properties of the resulting interface. Due to its high uniaxial magnetocrystalline anisotropy energy (MAE) of 7×10^7 ergs/cm³, the FePt-L1₀ alloy is a promising candidate for the next generation for the fabrication of ultra-high-density data-recording devices. FePt in the disordered state has a face-centered-cubic (fcc) crystal structure and is magnetically soft. In contrast, the ordered face-centered tetragonal (fct) L1₀ phase of the FePt alloy has Fe and Pt atomic planes stacked alternatively along the *c* axis in the equiatomic composition. On this phase it exhibits exceptional magnetic properties including high uniaxial (MAE), high coercivity, high saturation magnetization, and good chemical stability [5]. There have been a number of studies looking at the magnetic properties of FePt-L1₀, for example, in films or multilayers [6–8], slabs [9], and more recently in doped bulk phases [10].

However, during the past decade the possibility to use clusters deposited on surfaces to increase the recording density [11–14] has emerged. These clusters or nanoparticles (NPs) have different properties from bulk counterparts due to their reduced surface atomic coordination. In particular, binary 3*d*-5*d* NPs formed by transition metals, such as Fe or Co, together with 5*d* noble metals, such as Au or Pt allow the possibility to tune the magnetic properties based on an in-depth knowledge of their geometrical and magnetic behaviors [15–20]. The high MAE also permits the use of smaller particles before the onset of superparamagnetism, which may translate into potentially larger recording densities. Hence, the

primary motivation to synthesize and study perpendicularly oriented FePt nanoparticles dispersed in a nonmagnetic matrix is to combine favorable properties, which accompany size reduction, with superior magnetic properties of FePt and arrive at a system that is highly suitable for high-density perpendicular magnetic recording.

Wettability and material spreading are of key importance for many applications. At large scales, wetting or nonwetting plays an important role in, for example, oil recovery [21], and on a smaller scale, wetting solutions have been proposed to solve technological problems in microfluidics, nanoprinting, ink-jet printing, etc. [22]. All these phenomena are governed by the surface and interfacial interactions, acting usually at short (a few nanometers for van der Waals or electronic interactions) or very short molecular distances. These length scales are now being probed with relatively new experimental techniques, such as atomic force microscopy, or theoretical tools, such as molecular dynamics [3,23]. In such surface-anchored cluster/alloy systems it would be highly desirable to find ways to control and tune the properties of the adsorbed clusters through manipulation of the supporting substrate and the deposited clusters. The properties that may be influenced via substrate manipulation include: adsorption energies, cluster geometries and dimensionalities, cluster diffusion barriers, charge distributions, and chemical reactivities.

The magnetic properties of gas-phase metal clusters have been the subject of both experimental and theoretical investigations as we have pointed out, however, here we study the wettability of the FePt-L1₀ alloy onto a MgO surface. The growth of FePt on MgO has been predicted to be one of the possible candidates for the fabrication of ultra-high-density data-recording media. Thus, in this study, we have performed detailed density functional theory (DFT) computations to study the adsorption of bimetallic Fe_xPt_y clusters on MgO, where $x + y \leq 4$. We present the study of the structural, electronic, and magnetic properties of these ultrasmall clusters regarding different adsorption sites for the Fe or Pt species, namely, @*top*-O/-Mg and @*hollow* sites. Even though the

size of these small aggregates is far from the real structures currently used as recording magnetic media, a look into the complicated bonding mechanism at the atomic level between Fe or Pt species with the MgO surface will elucidate the still unclear interplay between these ferromagnetic-oxide systems. The importance of how FePt-L1₀ grows onto MgO is of vital importance in magnetism because of the following questions: (1) What are the stable configurations for the adsorption of these Fe_xPt_y clusters on MgO? (2) How do the electronic and magnetic properties of the adsorbed clusters vary with the sizes? (3) How does the chemical activity of these functionalized MgO-by-Fe_xPt_y clusters progress?

The paper is structured as follows. In Sec. II we describe the theoretical tools to perform all the calculations as well as the set of geometries studied in the present paper. Convergence tests are presented in Sec. III A. The energetic and structural analysis after the relaxation of the *dimers*, *trimers*, and *tetramers* will be explained in Sec. III B. The *intracluster* and the cluster-to-surface charge-transfer study are described in Sec. III C together with the local magnetic moments (MMs) analysis. Finally, Sec. IV summarizes the main results.

II. THEORETICAL METHODS

Our density functional based calculations have been performed using the code SIESTA [24] within the generalized gradient approximation (GGA) for the exchange-correlation (XC) potential [25]. We used norm-conserving pseudopotentials in the separate Kleinman-Bylander [26] form under the Troullier-Martins parametrization [27], and to address a better description of the magnetic behavior, nonlinear corrections were included in the XC terms [28]. The valence reference electronic configurations for the pseudopotentials are $4s^2 4p^0 3d^6$ (Fe), $6s^1 6p^0 5d^9$ (Pt), $3s^2 3p^0 3d^0$ (Mg), and $2s^2 2p^0 3s^2$ (O) with *s/p/d* cutoff radii 2.0/2.5/0.6 a.u. (Fe), 2.0/2.75/1.25 a.u. (Pt), 2.6/2.6/2.6 a.u. (Mg), and 0.75/0.75/1.75 a.u. (O), respectively. The geometry optimizations were carried out using the conjugate gradient (CG) method on a spin-polarized scalar relativistic level. As a basis set, we have employed double- ζ polarized with strictly localized numerical atomic orbitals, and the electronic temperature— kT in the Fermi-Dirac distribution—was set to 50 meV. After the relaxation process the forces per atom were less than 0.03 eV/Å.

The adsorption of the Fe_xPt_y clusters onto a MgO surface has been modeled as a two-dimensional periodic slab comprising four MgO(001) layers. We first consider *dimer* structures as illustrated schematically in Fig. 1, followed by more complex FePt clusters as depicted in Fig. 2. The magnesium oxide structure can be described as two interpenetrating fcc lattices displaced by $a/2(111)$ along the body diagonal of the conventional cube, and the bulk experimental value for its lattice parameter is $a = 4.22$ Å. We optimized the MgO lattice constant a for the GGA-XC functional obtaining a lattice value of 4.30 Å. To converge the physical quantities and minimize the out-of-plane and in-plane interactions between nearest cells, a total of 32 in-plane MgO atoms was chosen as we will point out in Sec. III A.

In this paper, the adsorption energies E_{ads} were evaluated after subtracting from the total energy of each configuration of the energy of the clean MgO surface and those of the clusters

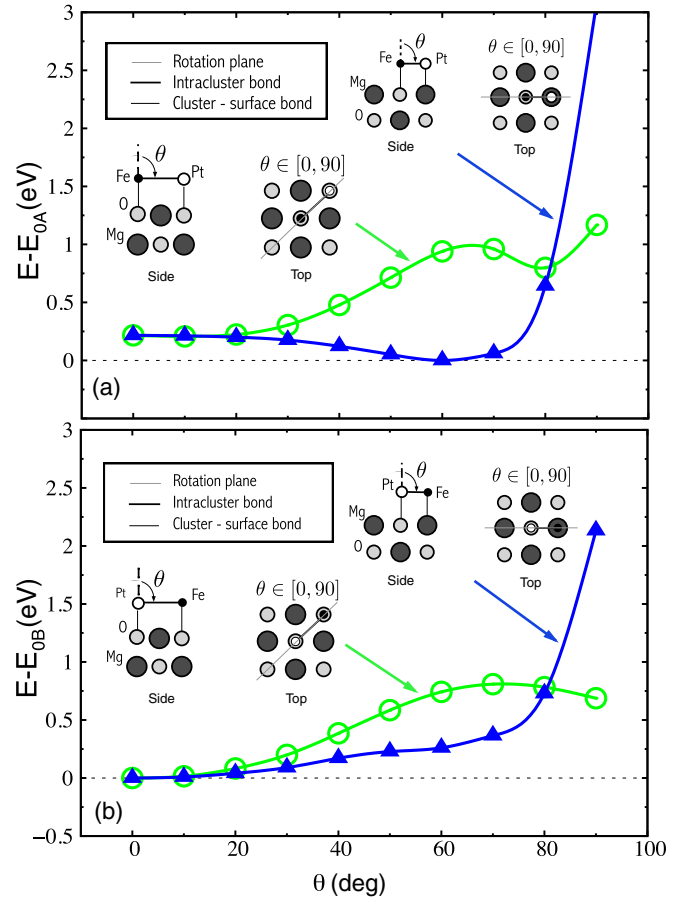


FIG. 1. (Color online) Variation in the total energy of a FePt dimer supported on a MgO surface with the angle of the dimer bond θ (measured from the normal to the MgO plane). In (a) the Fe side of the dimer is closer to the MgO surface, and the dimer is initially placed vertically. The scans take place on two different planes: (011) (full blue triangles) and on (101) (empty green circles). In (b) the Pt atoms are placed closer to the surface, and the scans are carried out as in (a). In both figures the total energies are plotted relative to the minimum energy for each arrangement (E_{0A} and E_{0B}). The solid lines are a guide for the eye.

in the following equation:

$$E_{\text{ads}} = -(E^T - E_C^T - E^{\text{at./clus}}),$$

where E^T is the total energy of the whole system, E_C^T is the energy of the clean MgO surface, and $E^{\text{at./clus}}$ is the energy if either one Fe/Pt atom or Fe_xPt_y clusters are adsorbed.

III. RESULTS AND DISCUSSION

We performed an energetic study of different size FePt clusters adsorption on the MgO(001) surface. Several adsorption sites and cluster orientations with respect to the MgO surface were taken into account. The optimized geometric configurations were obtained by means of the conjugate gradient method allowing that the clusters and the first two MgO layers moved freely. In the following we present the systematic analysis of the geometric, electronic, and magnetic properties of these

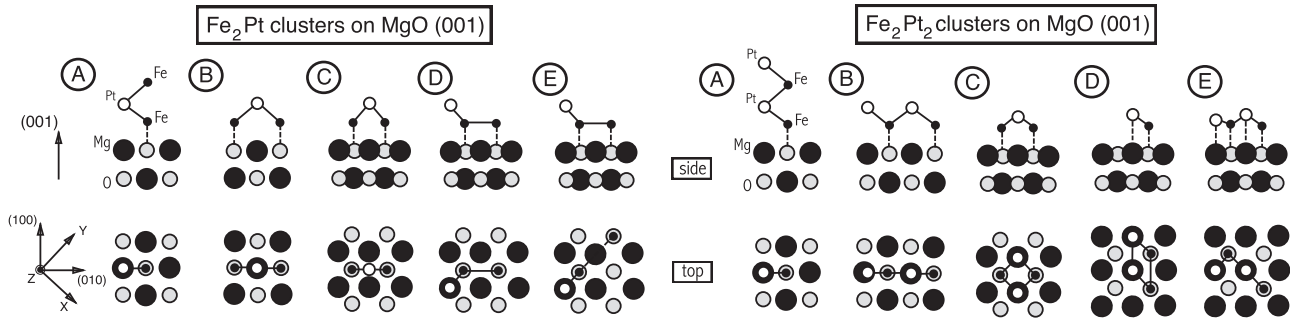


FIG. 2. Schematic of the initial configurations for the different adsorption positions of the Fe_2Pt and Fe_2Pt_2 clusters on the $\text{MgO}(001)$ surface, left (A–E) and right (A–E), respectively. The side (top) views are depicted in the upper (lower) row. In this schematic of the adsorption of the Fe_nPt_m clusters on the MgO surface only the Fe species are directly in contact with the surface via the O atoms. However, along the text, the study of the Pt species on the MgO surface has also been taken into account.

optimized configurations checking previously the feasibility of the calculations with a convergency test for two unit-cell sizes.

A. Convergence test

In order to use the best geometric configuration to avoid the spurious interaction between adjacent in-plane and out-of-plane cells due to the periodic boundary conditions, we have calculated the adsorption energy of one Fe and Pt atom on the $@top\text{-O}$, $@top\text{-Mg}$, and $@hollow$ sites as well as the vertical distances between these atoms and the MgO surface. In order to ensure that our model systems were sufficiently large we have investigated the effect of increasing the MgO system size. Specifically, we have chosen two supercell sizes labeled $c18$ and $c32$ with 18 and 32 MgO atoms, respectively, at the surface and varied the thickness of the supported MgO layer by varying the number of atomic planes from 2 to 5. Each configuration was optimized using the conjugate gradient (CG) method until the forces between atoms were less than $0.03 \text{ eV}/\text{\AA}$. The relaxations were undertaken allowing the Fe or Pt atoms and the first two MgO planes to move freely, keeping the atoms belonging to the last MgO layers fixed to their bulk sites. Only for the configurations in which the number of MgO planes were two or three, i.e., $c18/32\text{-}2/3$, and only the first MgO layer was allowed to move together with the adsorbed atoms. In Table I we can see the values of the adsorption energies (E_{ads}) and the heights between the Fe/Pt atoms and the surface ($z_{\text{Fe/Pt}}$). These values were computed as the difference in the z coordinate between the Fe/Pt and the O/Mg species, depending on whether the adsorption site was $@top\text{-O}$ or $@top\text{-Mg}$, respectively. The perpendicular distances for atoms situated on the $@hollow$ sites were calculated as the difference of the z coordinate of the Fe/Pt and the average z coordinate of O and Mg.

Detailed analysis of Table I is not germane to the aim of the paper, so here we only discuss the main results in order to discriminate the less accurate geometric configurations and define the best geometry for accurate and CPU efficient calculations of the properties of FePt clusters on MgO . We expect that a bigger supercell together with a higher number of MgO layers will provide more accurate calculations. The reason is clear after inspection of the differences in the E_{ads} as we move from two to five MgO layers and after we compare the values between the $c18$ and the $c32$ supercells. As an

example, in $c18\text{-Fe}@top\text{-O}$ configurations the E_{ads} converges to 2.32 eV as the MgO thickness increases. Almost the same value is achieved when the $c32$ was used (2.28 eV). This suggests that the use of the $c32$ configuration composed of four or five MgO layers is sufficient to study the adsorption of the FePt clusters onto the $\text{MgO}(001)$ surface. Beyond this there are no significant changes in the distances between the atoms and the surfaces, only around $\pm 0.05 \text{ \AA}$, in moving to the higher thicknesses and sizes.

TABLE I. Adsorption energies E_{ads} heights of the Fe/Pt adatoms with respect to the first MgO plane $z_{\text{Fe/Pt}}$ for the $top\text{-O}/\text{-Mg}$ and $hollow$ adsorption sites for different numbers of support MgO planes N_l and for two sizes of the unit cell: $c18$ and $c32$. The energies are in eV, and the heights are in angstroms.

| Cell | Fe/Pt site | N_l | Fe adatom | | Pt adatom | |
|-------|-----------------|-------|------------------|-----------------|------------------|-----------------|
| | | | E_{ads} | z_{Fe} | E_{ads} | z_{Pt} |
| $c18$ | $Top\text{-O}$ | 2 | 2.26 | 1.99 | 3.54 | 2.00 |
| | | 3 | 2.10 | 1.92 | 3.64 | 2.00 |
| | | 4 | 2.25 | 1.93 | 3.50 | 2.00 |
| | | 5 | 2.32 | 1.97 | 3.35 | 2.00 |
| | | 5 | 2.32 | 1.97 | 3.35 | 2.00 |
| | $Top\text{-Mg}$ | 2 | 0.69 | 2.87 | 1.63 | 2.64 |
| | | 3 | 0.87 | 2.70 | 1.44 | 2.60 |
| | | 4 | 0.71 | 2.73 | 1.91 | 2.65 |
| | | 5 | 0.67 | 2.75 | 1.16 | 2.64 |
| | | 5 | 0.67 | 2.75 | 1.16 | 2.64 |
| | $Hollow$ | 2 | 1.74 | 1.96 | 2.67 | 2.05 |
| | | 3 | 1.88 | 1.90 | 2.70 | 2.03 |
| | | 4 | 1.56 | 1.96 | 2.65 | 1.98 |
| | | 5 | 1.50 | 1.95 | 2.71 | 1.98 |
| | | 5 | 1.50 | 1.95 | 2.71 | 1.98 |
| $c32$ | $Top\text{-O}$ | 2 | 2.40 | 1.93 | 3.51 | 2.00 |
| | | 3 | 2.17 | 1.92 | 3.56 | 2.01 |
| | | 4 | 2.29 | 1.93 | 3.62 | 2.00 |
| | | 5 | 2.28 | 1.93 | 3.70 | 2.01 |
| | | 5 | 2.28 | 1.93 | 3.70 | 2.01 |
| | $Top\text{-Mg}$ | 2 | 0.84 | 2.97 | 1.35 | 2.57 |
| | | 3 | 0.87 | 2.92 | 1.86 | 2.67 |
| | | 4 | 0.88 | 2.94 | 1.53 | 2.64 |
| | | 5 | 0.88 | 2.91 | 1.53 | 2.66 |
| | | 5 | 0.88 | 2.91 | 1.53 | 2.66 |
| | $Hollow$ | 2 | 1.26 | 1.95 | 2.70 | 1.99 |
| | | 3 | 1.75 | 1.94 | 2.72 | 1.95 |
| | | 4 | 1.64 | 1.96 | 2.80 | 1.99 |
| | | 5 | 1.49 | 1.95 | 2.53 | 2.00 |
| | | 5 | 1.49 | 1.95 | 2.53 | 2.00 |

It is interesting to note that the Pt atoms prefer to lie @*top*-O as shown in the adsorption energies in comparison with the other adsorption positions and species in Table I. This is surprising because as shown in Ref. [29] the Fe atoms of a FePt-L1₀ alloy prefer to lie @*top*-O rather than having a Pt termination. Clearly the behavior of individual Fe and Pt atoms is very different from that of a FePt alloy on MgO(001). However, we will show later that as the size of the FePt clusters increases the preferential adsorption of the Fe species returns to the @*top*-O site after adding one Pt atom to the cluster.

B. DFT structural relaxations

The main purpose of this paper is to shed light on whether the magnetic FePt-L1₀ alloy prefers to grow vertically or horizontally when it is supported by the MgO(001) surface. If the magnetic alloy grows covering the whole surface, it is said that the FePt wets the MgO surface. In the other case the L1₀-like structure will cover the MgO surface forming FePt-L1₀ “drops.” The most obvious means of determining whether the FePt wets the MgO would be to simulate large extended structures to determine the preferential growth. However, such calculations would be extremely computationally expensive and beyond the scope of this paper. Instead, we have used only a representative number of ultrasmall Fe_xPt_y clusters with different sizes and structures, ranging *x* and *y* from 1 to 2. As we will see, we will fix some atoms of the clusters @*top*-O on the MgO surface and will move others in order to scan different adsorption positions, keeping the same number of the total atoms in the cluster. As we pointed out in Sec. III A we have used four MgO planes and the *c*32 supercell for all the calculations. The Fe_xPt_y clusters and the first two MgO planes were allowed to move freely during the optimization, keeping the atoms of the last two planes fixed at their bulk positions. The final forces on the atoms involved were less than 0.03 eV/Å.

1. Dimers on MgO

Figure 1 summarizes the total energy profile of the FePt dimer adsorbed onto the MgO surface as a function of angle θ . As the schematic adsorption geometries insets show in the figure, $\theta = 0^\circ$ corresponds to the first configuration, that is when the dimer lies just out of plane with respect to the MgO surface; the following total energy values were calculated at 10° intervals along circular trajectories on the (011) and (101) rotation planes, depending on whether the farthest Fe or Pt atom was conducted to lie @*top*-O (green empty circles) or @*top*-Mg (blue full triangles), respectively. This ensures that we checked two possible adsorption sites for the outermost atoms. In addition, and based on the convergence test in Sec. III A, we calculated two possible adsorption configurations depending on whether the Fe or Pt atoms lie @*top*-O, Figs. 1(a) and 1(b), respectively. Each calculation fixes the dimer bond value, and only the angle is changed at each step. To construct the $\theta = 0^\circ$ configuration, the distance between the O and the Fe or Pt atoms was optimized moving away and approaching the dimer to the surface. The minimum of the quadratic energy curve gives the Fe/Pt bond distance between the atoms and the O site.

Consider first the A arrangement where Fe is situated on @*top*-O. The dependence of *E* on the angle is shown for the cases of Pt moving towards the Mg and O sites. The rotation toward the @*top*-O site gives generally a monotonic increase, albeit with a local minimum close to 90° . The global minimum occurs for Pt rotating towards the top Mg site at an angle of around 60° . In comparison, the case B arrangement has a local minimum at 0° , i.e., with the dimer oriented perpendicular to the MgO plane. We note that the energies are plotted relative to the minimum energy and that $E_{0A} < E_{0B}$. Thus the global minimum for all configurations occurs for the A arrangement with Pt rotated toward the Mg site.

In general, although in this case we only have a dimer on MgO and we are far from the FePt bulk phase, we note that the angle is close to the FePt-L1₀ bulk phase ($\approx 46^\circ$). This is an attempt to discriminate how the FePt-L1₀ grows onto the MgO alloy.

2. Trimers and tetramers on MgO

In the next step we increase the number of atoms in the FePt cluster to three, four, and so on. Figure 2 shows the schematics of the initial Fe₂Pt (left) and Fe₂Pt₂ (right) adsorbed clusters onto the MgO(001) surface. In both cases we have labeled them from A to E, although it should be noted that they appear in no particular order. In the picture we only show the configurations in which the Fe atoms are fixed to the O sites. Those in which the Pt atoms are fixed in the same way as the Fe have also been studied, but they are not shown in Fig. 2. The furthest Fe(Pt) atom from the surface in Fe₂Pt(Fe₂Pt₂) was placed at several adsorption sites on the surface in order to scan the total energy dispersion and enable us to discriminate the preferential growth type of FePt-L1₀ onto the MgO alloy.

Among all the configurations, A would represent a vertical growth, whereas the others correspond to the FePt atoms wetting MgO. Within the four B–E geometries we will discriminate how far the Fe/Pt species prefer to lie from each other while the FePt alloy grows. For instance, in the Fe₂Pt B and C geometries, the Pt atom is located on the @*top*-Mg or @*hollow* site, respectively. The remaining two settings accommodate the second Fe closer (D) or farther (E) from the first Fe fixed @*top*-O. Similar situations are depicted for tetramers (B–E). The starting configurations for the trimer were constructed as follows: Keeping the best dimer geometry, i.e., 60° , we added one more atom further away from the surface in A and at different sites for the remaining places (B–E). It is worth mentioning that, as we showed earlier in Sec. III B1, when the Pt atom was closer to the O site the best configuration was vertical, so we would expect the lowest energy to be obtained by adding the next Pt to this dimer. However, since we want to compare quantitatively the total energies of similar geometries, initially we placed this additional Pt atom at the same position as the previous one. In the case of the tetramer we had to proceed more carefully because more initial configurations were possible. In order to reduce them we just inspected some. In Fig. 2(left) configuration A, we added one Fe/Pt atom following the usual construction of a hypothetical FePt-L1₀ unit cell. In the remainder we only placed the Fe/Pt at different sites. Again it must be pointed out that additional possibilities will arise when

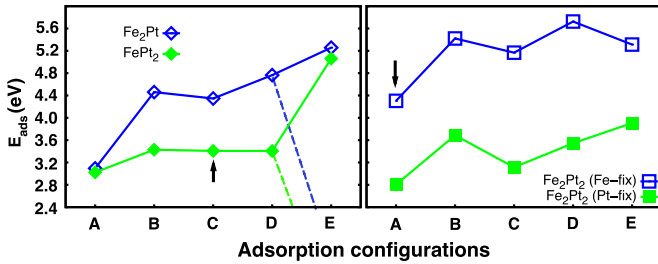


FIG. 3. (Color online) Different adsorption positions prior to the adsorption energy. Left: Fe_2Pt and FePt_2 trimers, blue empty and filled green diamonds, respectively. The blue and green dashed lines represent the hypothetical link between the D and the E configurations after subtracting the adsorption energy of the isolated Fe or Pt atom; right: Fe_2Pt_2 tetramers, blue empty and green filled squares represent whether the first contact atom is Fe or Pt, respectively. The black arrows show two configurations that changed substantially after the relaxations.

the number of atoms increases, but the aim of the present study is to have an initial indication of how the FePt “covers” the MgO so that a few reasonable geometries would in principle be enough.

After the relaxation, the shapes of all the initial geometries were kept, just some of the atoms in FePt_2 -C and Fe_2Pt_2 -A (Fe terminated) moved away from their initial sites. These structures are marked in Fig. 3 with black arrows. In the first case, the Fe located @hollow initially, moved to lie just @top-Mg, and in the second, the initial geometry is broken having finally each Pt atom @top-O/Mg keeping the Fe atoms @top-O.

In principle, the higher the adsorption energy, the more stable the structure. In this respect, we observe that the $\text{FePt}_2/\text{Fe}_2\text{Pt}$ -E geometries correspond to the highest E_{ads} and they should be the most stable. However, we have to take into account that in the trimer-E cases one of the Fe/Pt atoms is located farther away with respect to the other FePt structures and it could be treated as an “isolated” atom added to the dimers. So, as we pointed out in Table I, whether one Fe or Pt atom is adsorbed onto a $c32$ supercell using four MgO planes the E_{ads} takes the values of 2.29 eV for Fe and 3.62 eV for Pt. Roughly, we can subtract these values from those in Fig. 3, and we would get the values of ≈ 2.0 eV for FePt_2 and ≈ 1.5 eV for Fe_2Pt . This immediately would indicate that these configurations would not belong to those preferential geometries for the FePt on MgO and we can discard them from the preferential growth modes. We justify this conclusion by comparing the distances between Fe/Pt pairs in E and the other configurations. In E, the Fe-Fe distance is 4.3 and 4.71 Å for Pt-Pt. The calculated Fe-Fe bond distance for the other geometries is around 2.4 and 2.8 Å for the Pt-Pt. Furthermore, if we focus on, for example, the B configuration that has a mediated Fe or Pt atom, the distances are 4.1 and 3.7 Å for Fe-Fe and Pt-Pt, respectively. In Fig. 3 the blue and green dashed lines represent the connection between the D and the E adsorption energies in the case that we would assume the previous behavior. It is then interesting to note that the three B, C, and D geometries have almost similar adsorption energy values indicating that the trimers preferentially spread

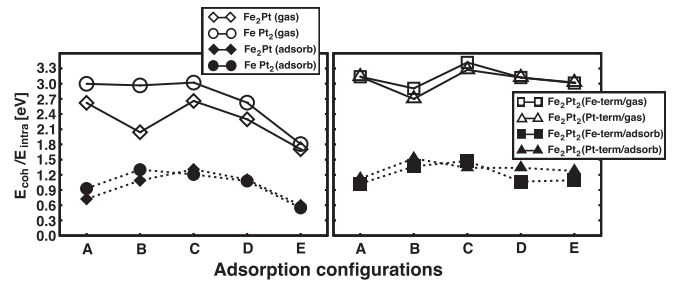


FIG. 4. Cohesive (gas phases) and intracuster binding energies (supported) as a function of the different adsorption positions for the trimers and tetramers, left and right graphs, respectively. Empty symbols depict the E_{coh} for the clusters after removing them from the MgO surface, and the filled ones depict the intracuster energy after the adsorption.

on MgO instead of growing vertically. As we pointed out, the preferential adsorption is when Fe atoms are closer to the MgO as the blue line shows.

The E_{ads} for the tetramers shown in Fig. 3(right) tends to corroborate our argument from the previous paragraph, namely, that from the B up to the E geometries the adsorption energies increase with respect to A, indicating a predisposition of the Fe/Pt atomic species to lie onto MgO, covering the surface. It is worth nothing that the E configuration for trimers is not present for tetramers due to the fact that we scanned a limited number of geometries as we pointed out before. The blue line in Fig. 3(right) shows that the tetramers follow the same trend as the trimers, having the higher adsorption energies to those for which the Fe atoms are in contact with the Mg surface. We observe in B–E an oscillation in the E_{ads} , but its dispersion is only about 0.5 eV. An additional study of the geometry as, for example, the bond and angle distances would explain the origin of this oscillation, but this study is beyond the scope of the current paper. However, we will compare the cohesive energy of the clusters in their gas phases with respect to those adsorbed onto the MgO surface in order to check the stability.

In Fig. 4 is shown the cohesive and intracuster binding energies of each cluster adsorbed at different i sites before and after the adsorption onto the MgO surface, empty and filled symbols, respectively. The comparison of these binding values will give an idea of the stability of the clusters upon the adsorption and which of them presents more stability at the surface. The binding energies were calculated in the following equations:

$$E_{\text{coh}}^G(i) = -[E_{G,i}^T - n_{\text{Fe}}E_{\text{Fe},i}^{T,G} - n_{\text{Pt}}E_{\text{Pt},i}^{T,G}]/N,$$

for the gas phases (G) and by

$$E_{\text{intra}}^A(i) = -[E_{A,i}^T + (N-1)E_{C,i}^T - n_{\text{Fe}}E_{\text{Fe},i}^{T,A} - n_{\text{Pt}}E_{\text{Pt},i}^{T,A}]/N,$$

after the adsorption (A). $E_{G,i}^T$ is the total energy of the free cluster, $E_{A,i}^T$ is the total energy of the system upon the adsorption, $E_{C,i}^T$ is the total energy of the clean MgO surface, $E_{\text{Fe/Pt},i}^{T,G}$ is the total energy for an isolated Fe or Pt atom, $E_{\text{Fe/Pt},i}^{T,A}$ is the total energy for the surface on which the Fe or Pt atom is adsorbed, $n_{\text{Fe,Pt}}$ are the numbers of each

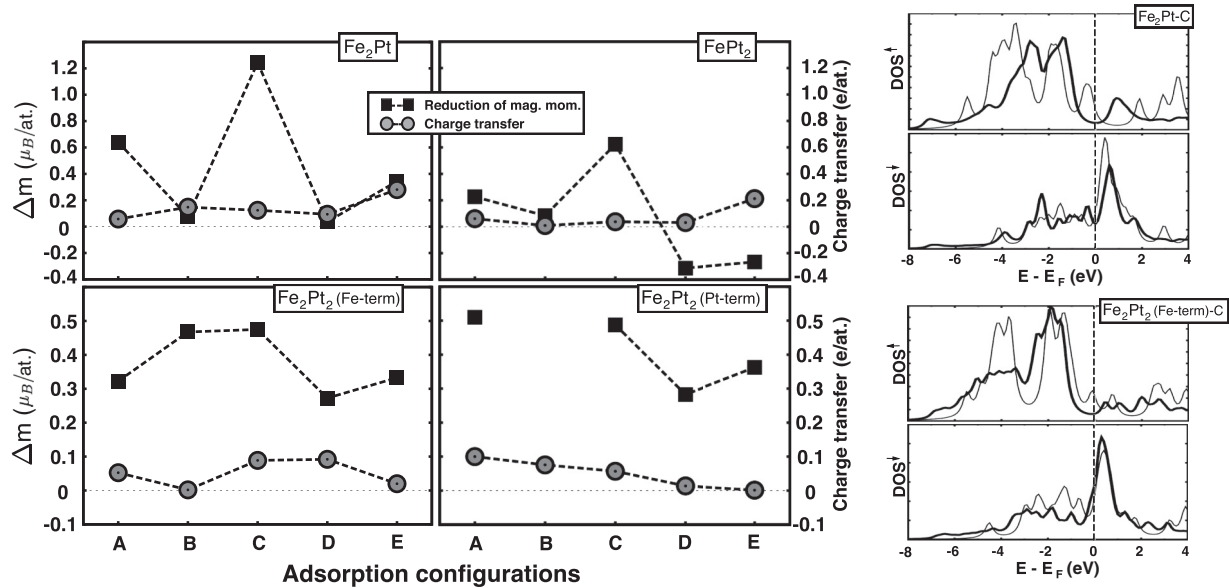


FIG. 5. Left: reduction of the magnetic moment $\Delta\text{MM} = \text{MM}^G - \text{MM}^A$ per atom (black squares) and charge transfer per atom (gray circles) as a function of the A–E geometries for *trimers* (first row) and *tetramers* (second row). Right: spin-up (down) projected density of states (DOS^\uparrow) for the $\text{Fe}_2\text{Pt-C}$ and $\text{Fe}_2\text{Pt}_2(\text{Fe-term})\text{-C}$ configurations, upper and lower two figures, respectively. The thick solid line represents the projected DOS for the adsorbed clusters, and the thin solid lines represent those in the gas phases. The DOS units are as usual in states/eV.

specie in the cluster, and $N = n_{\text{Fe}} + n_{\text{Pt}}$ is the total number of atoms in the cluster. The values of the $E_{\text{Fe/Pt},i}^{T,A}$ were calculated after performing a self-consistent calculation and keeping the closest Fe or Pt atom @*top-O*/-Mg as they were in the final relaxed configuration in the *trimers* and *tetramers*. The total energy of the clean surfaces $E_{C,i}^T$ was calculated by removing the cluster from the relaxed structures.

It is clear that the clusters in their gas phases are more stable than those adsorbed onto the MgO surface since the energy has reduced by an average value of 1.5 eV for the *trimers* and 2.0 eV for the *tetramers*. In this respect the *tetramers* present a slightly higher stability as indicated by the fact that the bigger the cluster, the more stable the structure. There is no significant difference in the cohesive and binding energies depending on whether the Fe or Pt atom is in contact with the surface. In general, the most stable configurations after the adsorption are B and C for *trimers* and *tetramers*. As we pointed out, these geometries would correspond to an initial covering of the MgO (see Fig. 2). However it is worth mentioning that the competition between adsorption on the surface and cohesion among the atoms in the clusters is an important feature of the $\text{Fe}_x\text{Pt}_y/\text{MgO}$ system.

C. Charge analysis and magnetic moments

In this section we address the Mulliken population analysis of each configuration to identify any charge transfer between the cluster and the surface atoms. The MM values were obtained by subtracting the spin-up from the spin-down populations. As we will see, upon adsorption, the net MM values of the *dimers* and *trimers* are reduced compared to the gas phases. The mechanisms that promote this change have two different origins: geometric and electronic. A rearrangement of the atoms in space after the ionic relaxation would imply a variation in the population of the cluster's states changing

the net MM values. However, after comparing the initial and final geometries there were no significant changes in the shape of the clusters, so we argue that the geometric disposition of the atoms does not influence the MM values too much so that the dominating contribution is most likely purely electronic. We separate the electronic part into two contributions: The first one sets up a charge transfer from the cluster to the surface, depopulating its states. The second, an *intracluster* rearrangement of the spin-up and spin-down charges internally increases the up or down population at the expense of the other. The gas phases of the adsorbed clusters present higher values of their total MM than those upon adsorption. Figure 5 presents, on the left, a reduction in the MM values (full black squares) for the *trimers* and *tetramers* (upper and lower rows, respectively) as a function of the A–E geometries. The total charge transfer per atom from the clusters to the surface (gray filled circles) is also shown. On the right we have plotted the up and down DOS for the $\text{Fe}_2\text{Pt-C}$ and $\text{Fe}_2\text{Pt}_2(\text{Fe-term})\text{-C}$ geometries as representative examples. As we distinguish in the figure, not all the configurations after the adsorption present this reduction, in particular $\text{Fe}_2\text{Pt}(\text{B,D})$ and $\text{Fe}_2\text{Pt}_2(\text{A,B})$. The reduction will be a complex balance due to the *intracluster* spin-up/-down charge transfer and the surface-to-cluster charge transfer.

The reduction of the MM is not principally caused by the charge flowing between the cluster and the surface in all the cases, but it is due to the *intracluster* electron displacements as well. On the right, the DOS^\uparrow for the $\text{Fe}_2\text{Pt-C}$ and $\text{Fe}_2\text{Pt}_2(\text{Fe-term})\text{-C}$ configurations show a hump below the Fermi level for the gas phases (gray thin solid line) around -0.5 eV for the first case and at -0.2 eV for the second. Upon adsorption these peaks move to the conduction band, implying a reduction in the up states. Part of this charge moves to the O sites and passes internally to the down states. The down states of the adsorbed clusters show a slightly different shape in the DOS compared to those in the gas phases. As we demonstrated

TABLE II. MM values in $\mu_B/\text{at.}$ of all the clusters deposited onto the MgO(001) surface as well as those obtained for the corresponding bulk alloys. The first column displays the adsorption configurations A–E as well as the bulk. The MM values in the first and second columns of each kind of adsorbed geometry have been calculated by means of the equations MM_M/N_M and MM_{NM}/N_{NM} , respectively, whereas in the text, M refers to the magnetic atoms and NM refers to the nonmagnetic ones. The third column shows $MM_{\text{tot}}/N_{\text{tot}}$.

| Configuration | Fe ₂ Pt | | | FePt ₂ | | | Fe ₂ Pt ₂ (Fe-term) | | | Fe ₂ Pt ₂ (Pt-term) | | |
|--------------------------|--------------------|------|-------------|-------------------|------|-------------|---|------|-------------|---|------|-------------|
| | M | NM | Total | M | NM | Total | M | NM | Total | M | NM | Total |
| A | 3.53 | 0.84 | 2.63 | 4.09 | 0.54 | 1.72 | 3.55 | 0.41 | 1.98 | 3.63 | 0.33 | 1.98 |
| B | 3.64 | 0.65 | 2.64 | 4.12 | 0.82 | 1.92 | 3.39 | 0.60 | 2.00 | 3.72 | 0.30 | 2.01 |
| C | 2.97 | 0.30 | 2.08 | 3.77 | 0.16 | 1.36 | 3.36 | 0.61 | 1.99 | 3.85 | 0.18 | 2.01 |
| D | 3.61 | 0.67 | 2.63 | 3.85 | 0.53 | 1.63 | 3.44 | 0.52 | 1.98 | 3.73 | 0.31 | 2.02 |
| E | 3.67 | 0.56 | 2.63 | 3.83 | 0.11 | 1.35 | 3.50 | 0.46 | 1.98 | 3.69 | 0.33 | 2.01 |
| Bulk ^a | 3.12 | 0.18 | 1.65 | | | | | | | | | |
| Bulk-others ^b | 2.96 | 0.34 | 1.65 | | | | | | | | | |

^aReference [30].

^bReference [31].

the charge balance between the cluster and the surface is quite complicated, nonetheless our data allow a useful initial attempt to explain its behavior.

In Table II we summarize the MM/at. values of all the configurations for the magnetic and the nonmagnetic species of the clusters as well as the total value in bold in the third column of each type of cluster configuration. For the *trimers*, the Fe₂Pt-*i* configurations have higher MM values than those of the FePt₂-*i* due to the presence of two magnetic atoms instead of only one. The Fe₂Pt shows the same MM values except for the C configuration that has $0.56\mu_B/\text{at.}$ lower. More significant is the change for FePt₂ whose MM value, depending on the adsorption site, can vary by up to $0.57\mu_B/\text{at.}$ Conversely the trimers present the same MM values for all the adsorption sites. Upon inspection of Table II and Fig. 3 we can conclude that there is no strong relationship between the magnetic behavior and the adsorption energies.

IV. CONCLUSIONS

We have performed an extensive survey of an ampler set of adsorption positions of the Fe_{*x*}Pt_{*y*} ($x, y \leq 1, 2$) ultrasmall clusters on MgO(001). To evaluate the preferential adsorption geometry of FePt on MgO we have calculated the energies associated with the adsorption of *dimers*, *trimers*, or *tetramers*. Furthermore, for each cluster size and shape we kept the Fe or Pt atom @*top*-O and moved the outermost ones onto several MgO sites. The schematics are depicted in Fig. 2. The structural analysis shows that the best adsorption geometries among all those studied are those in which they covered the surface avoiding vertical growth and thereby promoting

the wetting of MgO by FePt. After the adsorption, the *intracluster* energy has decreased by 1.5 eV, and the net MM reduces its values for all the configurations at the expense of a depopulation of the Fe up-*d* states, transferring part of this charge to the Pt atoms and externally to the O sites. We acknowledge that the charge balance as well as the E_{ads} are complex issues, however our study shows that the overall conclusion is that the FePt wets the MgO(001) surface. However, we also note that this is an initial study investigating the fundamental interaction potential between FePt and MgO. At nonzero temperatures the degree of wetting will be determined by a surface free energy, which requires molecular dynamics (MD) calculations and is beyond the scope of the current paper. However, the configurations studied here suggest a promising starting point for the calculation of the relevant *n*-body contributions to the FePt/MgO interaction potential which the MD calculations will require.

Finally, the complex charge-transfer processes at the FePt-cluster/MgO interface predicted here might be expected to be reflected in changes in the FePt MAE after the adsorption onto the MgO surface. However, this is an interesting possible effect, which is beyond the scope of the present paper but certainly worthy of further investigation.

ACKNOWLEDGMENTS

The authors are grateful to Dr. M. I. J. Probert, Dr. Y. K. Takahashi, and Dr. T. J. Klemmer for helpful discussions. Financial support from the EU Seventh Framework Programme under Grant No. 281043, FEMTOSPIN is gratefully acknowledged.

- [1] S. Sun, C. B. Murray, D. Weller, L. Folks, and A. Moser, *Science* **287**, 1989 (2000).
 [2] H.-J. Freund, *Surf. Sci.* **500**, 271 (2002).
 [3] V. Musolino, A. Selloni, and R. Car, *Phys. Rev. Lett.* **83**, 3242 (1999).

- [4] D. Ricci, A. Bongiorno, G. Pacchioni, and U. Landman, *Phys. Rev. Lett.* **97**, 036106 (2006).
 [5] D. Weller and A. Moser, *IEEE Trans. Mag.* **36**, 10 (2000).
 [6] J. Kohlhepp and U. Gradmann, *J. Magn. Magn. Mater.* **139**, 347 (1995).

- [7] C. J. Aas, P. J. Hasnip, R. Cuadrado, E. M. Plotnikova, L. Szunyogh, L. Udvardi, and R. W. Chantrell, *Phys. Rev. B* **88**, 174409 (2013).
- [8] J. Lindner, C. Rüdert, E. Kosubek, P. Pouloupoulos, K. Baberschke, P. Blomquist, R. Wäppling, and D. L. Mills, *Phys. Rev. Lett.* **88**, 167206 (2002).
- [9] R. V. Chepulska and W. H. Butler, *Appl. Phys. Lett.* **100**, 142405 (2012).
- [10] R. Cuadrado, T. J. Klemmer, and R. W. Chantrell, *Appl. Phys. Lett.* **105**, 152406 (2014).
- [11] O. Diéguez, M. M. G. Alemany, C. Rey, P. Ordejón, and L. J. Gallego, *Phys. Rev. B* **63**, 205407 (2001).
- [12] R. Cuadrado and R. W. Chantrell, *Phys. Rev. B* **86**, 224415 (2012).
- [13] P. Gambardella, S. Rusponi, M. Veronese, S. S. Dhesi, C. Grazioli, A. Dallmeyer, I. Cabria, R. Zeller, P. H. Dedrich, K. Kern, C. Carbone, and H. Brune, *Science* **300**, 1130 (2003).
- [14] G. M. Pastor, J. Dorantes-Dávila, S. Pick, and H. Dreyssé, *Phys. Rev. Lett.* **75**, 326 (1995).
- [15] G. Rollmann, M. E. Gruner, A. Hucht, R. Meyer, P. Entel, M. L. Tiago, and J. R. Chelikowsky, *Phys. Rev. Lett.* **99**, 083402 (2007).
- [16] L. Fernández-Seivane and J. Ferrer, *Phys. Rev. Lett.* **99**, 183401 (2007).
- [17] K. Chen, S. Fiedler, I. Baev, T. Beeck, W. Wurth, and M. Martins, *New J. Phys.* **14**, 123005 (2012).
- [18] Ž. Šljivančanin and A. Pasquarello, *Phys. Rev. Lett.* **90**, 247202 (2003).
- [19] V. Musolino, A. Selloni, and R. Car, *J. Chem. Phys.* **108**, 5044 (1998).
- [20] R. Ferrando, G. Barcaro, and A. Fortunelli, *Phys. Rev. B* **83**, 045418 (2011).
- [21] E. Bertrand, D. Bonn, D. Broseta, N. Shahidzadeh, K. Ragil, H. Dobbs, J. O. Indekeu, and J. Meunier, *J. Pet. Sci. Eng.* **33**, 217 (2002).
- [22] P. Tabeling, *Introduction to Microfluidics* (Oxford University Press, Oxford, 2011).
- [23] M. Alfredsson, C. Richard, and A. Catlow, *Surf. Sci.* **561**, 43 (2004).
- [24] J. M. Soler, E. Artacho, J. D. Gale, A. García, J. Junquera, P. Ordejón, and D. Sánchez-Portal, *J. Phys.: Condens. Matter* **14**, 2745 (2002).
- [25] J. P. Perdew, K. Burke, and M. Ernzerhof, *Phys. Rev. Lett.* **77**, 3865 (1996).
- [26] L. Kleinman and D. M. Bylander, *Phys. Rev. Lett.* **48**, 1425 (1982).
- [27] N. Troullier and J. L. Martins, *Phys. Rev. B* **43**, 1993 (1991).
- [28] S. G. Louie, S. Froyen, and M. L. Cohen, *Phys. Rev. B* **26**, 1738 (1982).
- [29] R. Cuadrado and R. W. Chantrell, *Phys. Rev. B* **89**, 094407 (2014).
- [30] R. Cuadrado and J. I. Cerdá, *J. Phys.: Condens. Matter* **24**, 086005 (2012).
- [31] I. Galanakis, M. Alouani, and H. Dreyse, *Phys. Rev. B* **62**, 6475 (2000).